Chapter 3

Alloy surface segregation and ordering phenomena: recent progress

M. Polak and L. Rubinovich

Department of Chemistry, Ben-Gurion University of the Negev,
Beer-Sheva 84105, Israel

1. OVERVIEW

Theoretical and experimental studies of surface segregation equilibrium phenomena in metallic alloys have been focused traditionally on substitutional solid solutions with elemental constituents (and non-metal impurities) assumed to be randomly distributed among the crystal lattice bulk and surface sites. Only in recent years more attention have been paid to the role of compositional order in surface segregation [1].

Ordering in alloys can be classified according to its range as short-range order (SRO) or long-range order (LRO), and is manifested in diverse structures. The sign and magnitude of the interatomic interactions are key factors in the compositional structural nature of equilibrium bulk phases in a multi-element (binary, ternary, etc.) system formed as function of temperature and overall composition (documented as phase-diagrams). In particular, in case of effectively attractive interactions between two elements, A and B, of a binary alloy,

$$V \equiv V^{AB} = \frac{1}{2}\left(u^{AA} + u^{BB} - 2u^{AB} \right) > 0 \qquad (1)$$

(u^{AA}, u^{BB} and u^{AB} being the interaction energies between the corresponding atoms), the formation of ordered metallic phases is quite common ("chemical" or "intermetallic" compounds with fixed composition, or alloys with a certain range of concentrations). In such ordered alloys atoms of one element tend to be surrounded by atoms of the other element in periodic crystal sub-lattices (Fig.1). At finite temperatures LRO is never perfect, and in addition, there are local fluctuations in composition, known as short-range order (SRO, see Fig.2),

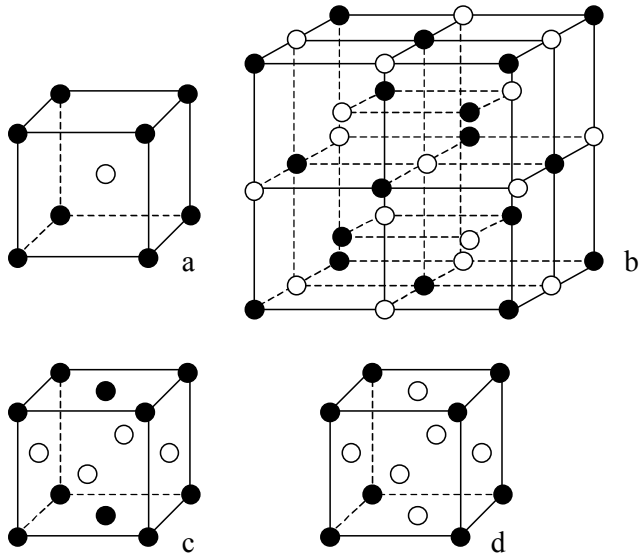

Fig. 1. Schematic view of the bulk unit cells of B2 (a), B32 (b), $L1_0$ (c) and $L1_2$ (d) binary ordered alloy structures. The two atomic sublattices are denoted by solid and open circles.

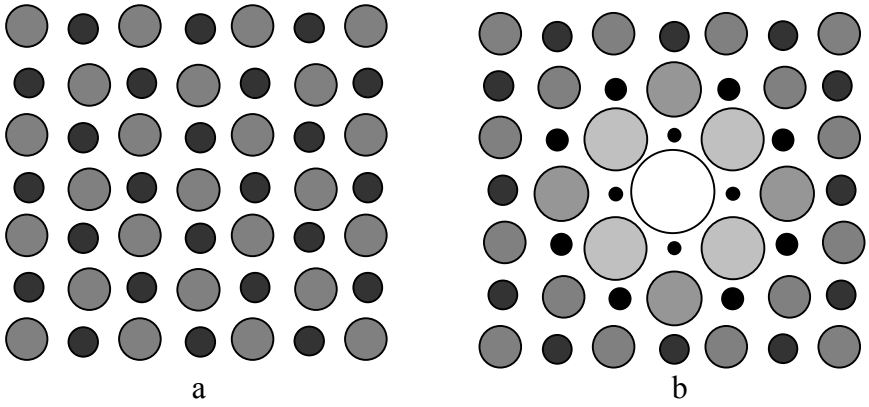

Fig. 2. 2D schematics of a binary ordered alloy crystal with LRO alone (a), and with LRO accompanied by short-ranged compositional fluctuations (b). The probability of finding atom A (or B) at a lattice site is expressed by means of the circle size (and colour): higher probability corresponds to larger (and brighter) circles. The largest white circle in (b) represents 100% probability.

which unlike LRO does not vanish at the order-disorder transition temperature.

In case $V < 0$, bonding of like atoms is energetically preferred, leading in principle to separation of the alloy into a mixture of A and B rich solid-solution phases, each with nearly homoatomic SRO clusters, compared to short range A-B mixed or heteroatomic clusters in the former case of $V > 0$. In other words, the tendency to order (or phase-separate) is manifested to some, local degree also in most solid solutions, where the distribution of atoms in the crystal is not entirely random, and should be incorporated too in any theoretical quantitative evaluation of surface segregation phenomena. Moreover, many alloys of

practical importance are comprised at temperatures below solubility limits of two or more phases in a certain micro- (or nano-) structure with ordered regions or clusters (characterized by LRO and SRO) embedded in solid-solution matrixes (with SRO). Since not only the LRO and SRO contributions are temperature dependent, but also the solid solution bulk compositions and relative amounts of phases (each with its distinct surface segregation behaviour), the segregation characteristics of such a multi-phase alloy surface can be even more complex than the single-phase cases.

Surface segregation of an alloy constituent, which is very common in substitutional (and interstitial) solid solutions, is expected to be manifested to a less extent in ordered alloys [1]. Thus, the process of segregation in A-B alloys, whereby atoms of one constituent element populate preferentially the surface layer, can be viewed as a sort of near-surface phase separation, which is typically incompatible with ordering tendencies*. Actually, segregation is expected to disrupt order and break energetically favourable A-B bonds, and hence as an endothermic process in strongly ordered systems, it may not occur at all, at least at relatively low temperatures. At higher temperatures this suppression is expected to diminish, as entropy-driven segregation with progressively higher levels prevails, until in case of a transition to a disordered phase, it becomes maximal usually around the range of the transition temperature (Fig.3). Then, in the solid-solution high temperature regime, the segregation level eventually decreases with temperature as an exothermic process. The resultant peaked segregation vs. temperature curve expected under certain conditions in strongly ordered systems has been predicted for alloys with LRO [2] and solid-solutions with strong SRO [3], and observed experimentally in several cases (e.g., Refs.3-5). The interplay of LRO and segregation can lead to other types of segregation curves, as described in section 3. Another complication, worthwhile mentioning in the context of developing insight into phenomena of surface segregation in the presence of ordering tendency, emerges when V is strongly composition dependent [6,7], or even changes sign, as in the case of the Fe-Cr system [8,9].

Describing of the *equilibrium state* of the macroscopic system by means of a statistical-mechanical approximation or Monte-Carlo (MC) simulations is one of the two main aspects of surface segregation theory, while the second aspect deals with the segregation *energetics* related to "microscopic" atomic interactions. Early experimental data on surface segregation phenomena in solid solutions were usually analyzed by means of the Langmuir-McLean theory [10]. This simplistic approach predicts monolayer segregation that decreases monotonously with temperature, and enabled to derive "segregation enthalpy"

* Yet, as discussed in Sec.3, in certain bulk truncated terminations of ordered alloys the two tendencies can be compatible.

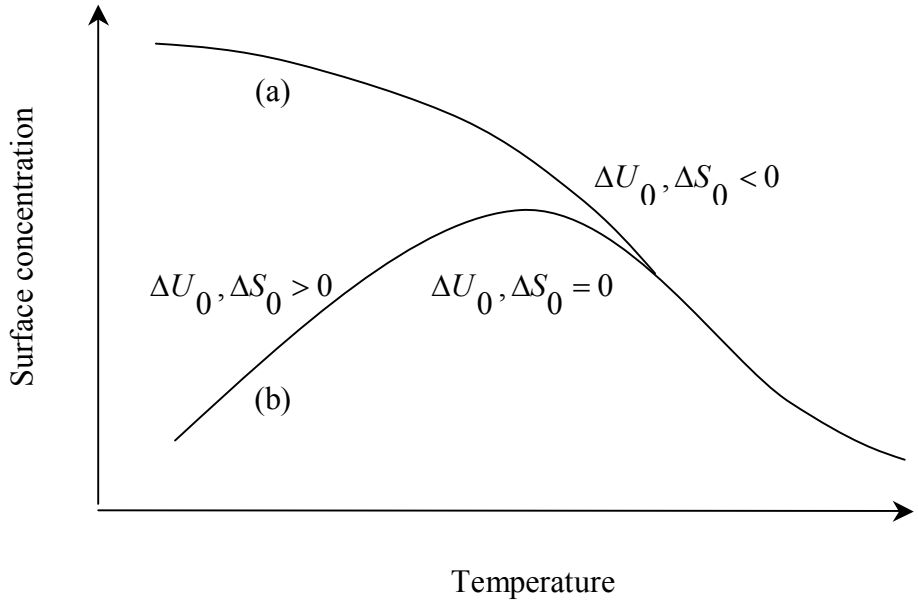

Fig.3. Schematics of the evolution of equilibrium segregation with temperature in alloys with order-segregation competition: (a) dominant surface segregation tendency (Langmuir-McLean behaviour), (b) dominant ordering tendency. Signs of enthalpy and entropy of segregation are indicated.

and "excess entropy" from experimental surface compositions vs. temperature (Fig. 3), but fails to account for the above mentioned complex segregation in alloys with interaction-induced strong ordering tendencies. Hence, together with the development of experimental techniques and the fast increase of relevant data, more elaborate theoretical approaches to surface segregation phenomena became necessary [1]. A better starting point for theoretical studies of LRO/segregation interrelations [11,12] became the Bragg-Williams (BW) statistical-mechanical approximation adapted for multilayer surface segregation while still assuming random distribution of atoms at identical layer and sub-lattice sites. It is based on Ising type rigid lattice model with constant bond energies, ignoring surrounding-dependent pair bonding and many-body interactions (an Ising type model that does consider composition dependent local interactions was introduced recently [9]). As further steps, basic SRO effects on surface segregation were treated by means of the statistical-mechanical cluster variation method (CVM) [13-18], and the free-energy expansion methods (FCEM, described in the next section) [1,3,9,19,20]. On the other hand, Monte-Carlo simulation methods [21-38] are capable of taking into account such contributions as atomic vibrations and surface atomic relaxation [29]. When combined with the embedded atom method (EAM) [23-25] as an improved energy model, or its modified version (MEAM) [37,39,40], MC simulations overcome several drawbacks of the above Ising type models. Yet,

the latter analytical approach can be helpful in predicting basic effects of atomic long-range and short-range order on surface segregation in alloys, including multi-component and dilute systems.

This chapter is focused on the most recent theoretical and experimental efforts aiming at unravelling the diverse phenomena of segregation/ordering interplay. The issue was reviewed by us comprehensively about two years ago [1], and new topics are addressed here in three separate sections:

(i) Theoretical formulation of multi-layer segregation in a multi-element solid-solution alloys (ternary alloys in particular) with emphasis on the role of short range order. It is followed by model calculations for Ni-Al-Cu solid solution.

(ii) Evaluation of surface segregation trends for several classes of ordered alloy surface structures, including case studies, primarily in terms of segregation/ordering energetics. In view of the prominence of LRO effects, they constitute a central topic in this review.

(iii) The complex segregation behaviour in a bi-phase system comprising of ordered clusters in a solid solution matrix.

2. SEGREGATION IN MULTI-ELEMENT ALLOYS

Compared to numerous studies of surface segregation phenomena in binary alloys [1,41], quite fewer studies have been devoted to the theory of surface segregation in multi-component (in particular, ternary) metallic alloys. Characteristic phenomena as co-segregation and site competition were addressed originally by Guttmann [42] using a regular solution model. Later, Wynblatt and Hoffmann [43] used a monolayer segregation model with more accurately approximated total free energy, and this formalism was modified to include the prediction of possible compositional phase transitions [44]. However, as mentioned above, a more accurate description demands taking into account short-range order (SRO), as well as *multilayer* segregation.

Free-energy approximate expressions that take into account SRO in the *bulk* of dilute binary [45,46], or multi-component [47] alloys were derived previously. However, their application to alloy *surfaces* is somewhat problematic, since upon segregation a solute can become a major constituent at the surface, thus violating the assumed low concentration. SRO correction for the binary alloy free energy, which is symmetric with respect to the alloy constituents, and thus overcomes this difficulty, was derived in the Ising model based "free-energy concentration expansion method" (FCEM) [1,3,19]. Being more accurate than the mean-field Bragg-Williams (BW) theory, and simpler to apply compared to the quasi-chemical and cluster variation methods, FCEM agreed quite well with MC simulations of segregation [19], while demanding much less computational efforts. Recently the FCEM approach was extended to

the case of alloys with any number of components [20]. An approximate SRO formula for multi-component alloy was constructed by adapting the corresponding binary alloy formula as a boundary case, and by making the multi-component alloy expression symmetric with respect to its components.

The FCEM expressions for binary alloys were obtained using the Ising model Hamiltonian and an expansion of the partition function and free energy in terms of solute concentration [1,3,19]. The free energy of a binary alloy (A - solute, S - solvent) reads,

$$\begin{aligned} F &= kT\sum_m \left(c_m^A \ln c_m^A + c_m^S \ln c_m^S \right) + \sum_m \Delta h_m^A c_m^A - \\ &+ \frac{1}{2} \sum_{\{mn\}} V_{mn}^{AS} \left(2c_m^A - 1 \right) \left(2c_n^A - 1 \right) - \\ &- \sum_{\{mn\}} kT c_m^A (1 - c_m^A) c_n^A (1 - c_n^A) \left(\exp\left(-2V_{mn}^{AS} / kT \right) + 2V_{mn}^{AS} / kT - 1 \right) \end{aligned} \tag{2}$$

where c_m^I is the concentration of a constituent I on a lattice site m, Δh_m^I denotes a layer "field" (assuming that the lattice site $m \in p$-layer), and V_{mn}^{IJ} is the effective pair interaction strength (see eq.1) between atoms of constituents I and J on lattice sites m and n. Rearranging the third term gives,

$$\frac{1}{2} \sum_{\{mn\}} V_{mn}^{AS} \left(2c_m^A - 1 \right) \left(2c_n^A - 1 \right) = - \sum_{\{mn\}} \left(V_{mn}^{AS} \left(c_m^B c_n^A + c_m^A c_n^B \right) \right) + \frac{1}{2} \sum_{\{mn\}} V_{mn}^{AS}$$

The last, constant term can be omitted, and contributions related to the interaction V_{mn}^{AS} in eq.2 can be rewritten in a form symmetric with respect to the constituent concentrations.

$$\begin{aligned} F &= kT\sum_m \left(c_m^A \ln c_m^A + c_m^S \ln c_m^S \right) + \sum_m \Delta h_m^A c_m^A - \\ &- \sum_{\{mn\}} \begin{pmatrix} V_{mn}^{AS} \left(c_m^A c_n^S + c_m^S c_n^A \right) + \\ + kT c_m^A c_m^S c_n^A c_n^S \left(\exp\left(-2V_{mn}^{AS} / kT \right) + 2V_{mn}^{AS} / kT - 1 \right) \end{pmatrix} \end{aligned} \tag{3}$$

Generalization of this formula to multi-component alloys is straightforward [20],

$$F = kT\sum_{m}\sum_{I} c_m^I \ln c_m^I + \sum_{m,\, I \neq S} \Delta h_m^I c_m^I -$$

$$- \sum_{\{mn\},\{IJ\}} \left(\begin{array}{l} V_{mn}^{IJ}\left(c_m^I c_n^J + c_m^J c_n^I \right) + \\ kTc_m^I c_m^J c_n^I c_n^J \left(\exp\left(-2V_{mn}^{IJ}/kT \right) + 2V_{mn}^{IJ}/kT - 1 \right) \end{array} \right) \qquad (4)$$

Pair probability of finding atoms of types I and J on lattice site m and n is given by the formula,

$$p_{mn}^{IJ} = c_m^I c_n^J + c_m^I c_n^I c_m^J c_n^J \left(1 - \exp(-2V_{mn}^{IJ}/kT) \right)$$

that coincides with the corresponding formula for a binary alloy [1,19].

In case of a ternary alloy (A,B - solutes, S - solvent) the free energy is given by,

$$F = kT\sum_{m}\left(c_m^A \ln c_m^A + c_m^B \ln c_m^B + c_m^S \ln c_m^S \right) +$$

$$+ \sum_{m}\left(\Delta h_m^A c_m^A + \Delta h_m^B c_m^B \right) -$$

$$- \sum_{\{mn\}} \left(\begin{array}{l} V_{mn}^{AB}\left(c_m^A c_n^B + c_m^B c_n^A \right) + \\ V_{mn}^{AC}\left(c_m^A c_n^S + c_m^S c_n^A \right) + \\ V_{mn}^{AB}\left(c_m^B c_n^S + c_m^S c_n^B \right) + \\ kTc_m^A c_m^B c_n^A c_n^B \left(\exp\left(-2V_{mn}^{AB}/kT \right) + 2V_{mn}^{AB}/kT - 1 \right) + \\ kTc_m^A c_m^S c_n^A c_n^S \left(\exp\left(-2V_{mn}^{AS}/kT \right) + 2V_{mn}^{AS}/kT - 1 \right) + \\ kTc_m^B c_m^S c_n^B c_n^S \left(\exp\left(-2V_{mn}^{BS}/kT \right) + 2V_{mn}^{BS}/kT - 1 \right) \end{array} \right) \qquad (5)$$

Formulas within the BW mean field theory are obtained by omitting the SRO related contributions containing $\left(\exp\left(-2V_{mn}^{IJ}/kT\right)+2V_{mn}^{IJ}/kT-1\right)$ from eqs.3-5.

The method was applied to the elucidation of effects of interatomic interactions and SRO on surface segregation in Ni-8%Al-4%Cu as a model ternary solid solution [20]. The results were then compared quantitatively to mean field calculations, and inspected in terms of the pertinent energetic parameters and effects of temperature. A primary consideration in choosing the Ni-Al-Cu system (Ni solvent) for model calculations was the relatively strong attractive Ni-Al interactions (which lead to significant SRO effects on surface segregation in Ni-9at%Al solid solution [1,3,19]). These effects are expected to be operative also in alloys containing a third constituent in low concentrations. Copper was chosen since Ni-Cu binary solid solutions (with quite weak repulsive interactions) had been extensively studied earlier and the corresponding energetic parameters are fairly known [48]. The energetics of the model was based on three nearest-neighbor (NN) interactions, V^{NiCu}, V^{NiAl} and V^{AlCu}, and two surface fields, Δh^{Al} and Δh^{Cu}, all listed in Table 1. In order to obtain the equilibrium layer compositions the free-energy (eq.5) was minimized numerically [20].

The alloy constituent concentrations calculated in the FCEM approximation for the first three atomic layers of the Ni-8at%Al-4at%Cu(111) surface are shown in Fig.4. A distinct surface phase transition characterized by a sharp jump in surface concentrations appears at 1075 K. Below this temperature the alloy surface is strongly Al depleted and Cu rich, while at the transition Al rises and Cu decreases, both reaching rather moderate segregation levels above it. The segregation behavior at all temperatures is indicative of site competition.

Table 1
Energetic parameters used in the model (in meV)

V^{NiCu}	V^{AlCu}	V^{AlNi}	Δh^{Cu}	Δh^{Al}
-12.5*	31**	136**	~120*	-570***

*Ni-Cu energetic parameters were taken from Ref.48; V^{NiCu} are enhanced at the surface by a factor of 1.5.

**Estimation obtained from the heat of mixing [49]

***The surface field Δh^{Al} for Ni-Al(100) has been determined as -680 meV [3], with -450 meV due to the difference in surface tensions [50]. Keeping the same elastic strain contribution, the estimation (-570 meV) takes into account the smaller number of (111) broken bonds per atom (3 vs. 4).

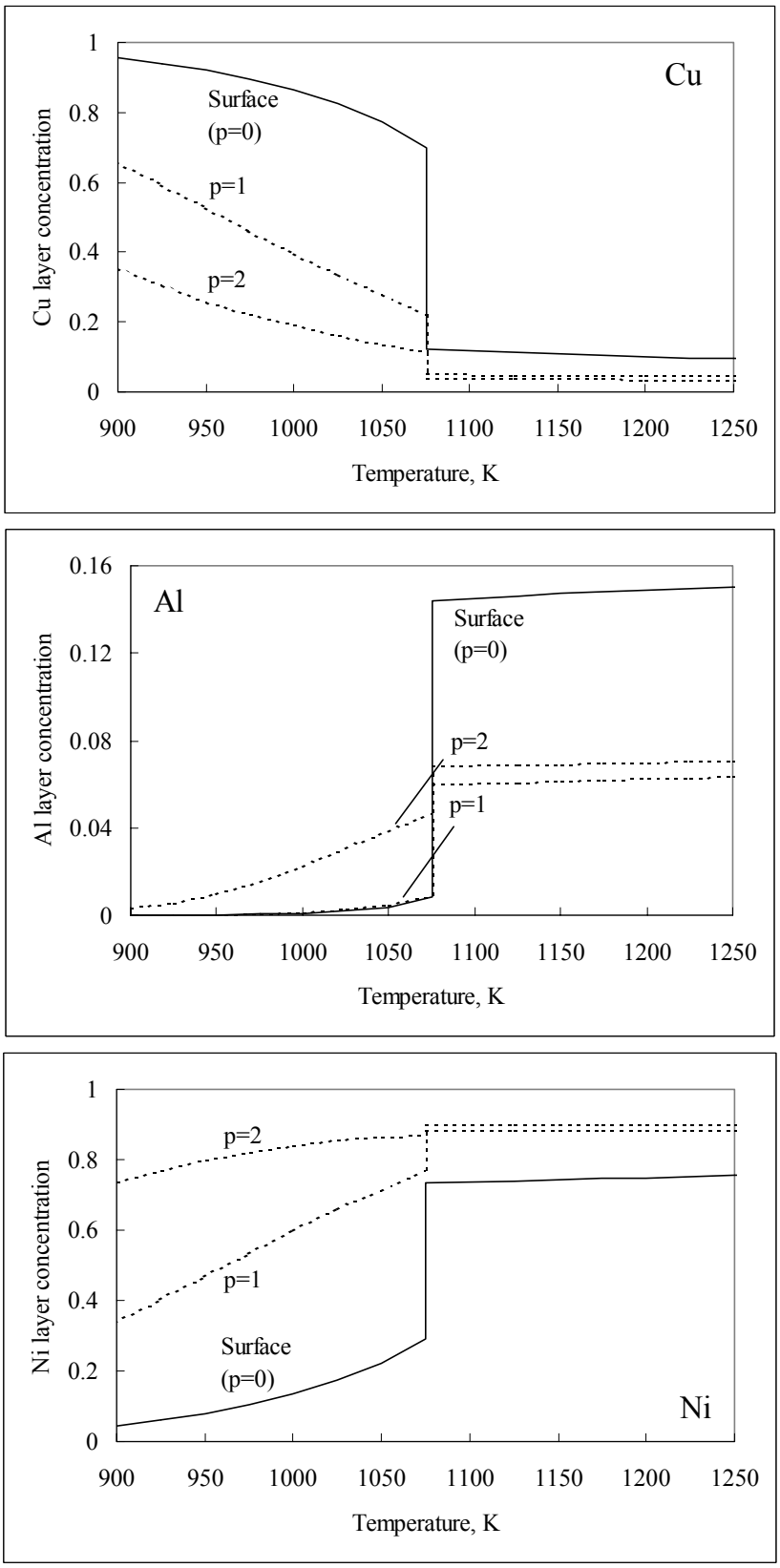

Fig.4. The near surface concentrations of fcc Ni-8at%Al-4at%Cu(111) calculated in the FCEM approximation. (p=1 and 2 correspond to the first and second under-layer, respectively.)

The predicted phenomena can be explained in terms of the different energetics and atomic coordination numbers involved. In particular, because of the reduced surface coordination, the Ni-Al prominent mixing tendency is stronger in the bulk, leading to diminished surface concentrations of these constituents ("co-desegregation") throughout the temperature range below the transition. Consequently, in spite of its lower surface field (Table 1) the overall effective driving force for Cu segregation in the ternary alloy is significantly stronger than for Al, and even at temperatures above the transition the (diminished) surface enrichment by Cu is higher.

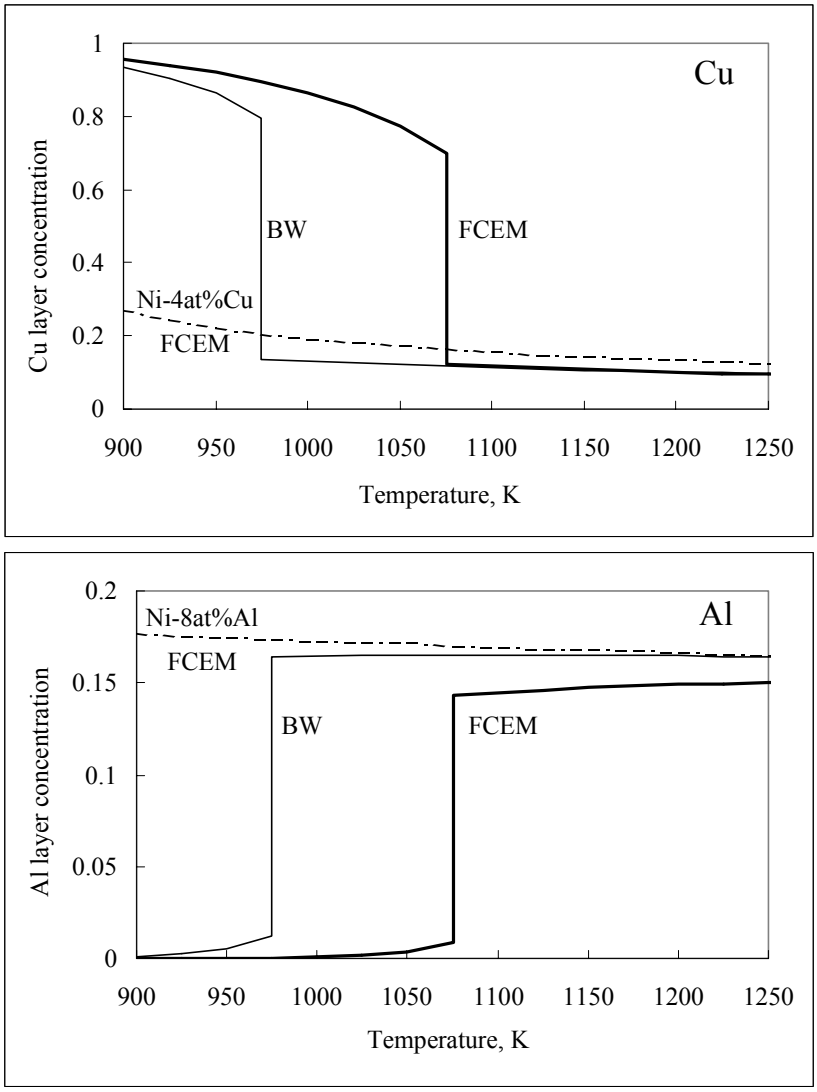

Fig.5. Calculated solute surface concentrations for Ni-8at%Al-4at%Cu(111): thick solid lines - FCEM, thin solid lines - the BW-type approximation. Dashed-dotted lines - solute surface concentrations for the binary alloy Ni-8at%Al(111) and Ni-4at%Cu(111) surfaces calculated in the FCEM approximation. Note the enhancement of Cu segregation induced by ternary alloying and short-range order effects.

The segregation of copper is further enhanced by short-range order that suppresses surface segregation of the solute (Al) interacting strongly with the solvent (Ni) [3,51]. Actually, SRO amplifies the interaction induced effects on segregation, without changing the general trend. Thus, as can be seen in Fig.5, the sharp transition in Cu surface concentration as predicted by the FCEM calculations occurs at a considerably higher temperature as compared to the results of the mean field (BW) theory that neglect interatomic correlations.

Furthermore, it can be expected that the Al-Ni strong mixing tendency which diminishes surface concentration of both these constituents in the ternary Ni-8at%Al-4at%Cu alloy, would promote Cu surface segregation far beyond the driving forces operative in the corresponding binary alloy Ni-4at%Cu. Conversely, Al segregation should be suppressed relative to its segregation levels in the binary Ni-8at%Al alloy. The FCEM results for the binary alloys, shown in Fig.5, indeed exhibit below the transition temperature Cu surface concentration much lower (and Al concentration much higher) than in the ternary alloy.

To summarize this section, the multi-layer FCEM calculations predict strong segregation of Cu associated primarily with the Ni-Al strong mixing tendency (attractive interactions) that effectively repels these constituents from the surface into the alloy bulk in an apparent site competition process. It appears to be operative also following a compositional phase transition, when the surface solute concentrations tend to be slightly *below* the respective binary alloy moderate segregation levels. Part of the former enhanced Cu surface segregation is associated with short range order effects that shift the transition to a higher temperature. These calculations can be further extended to other nominal compositions of this alloy, and the energetic parameters can be varied as to their general effects on site competition and surface phase transitions in ternary alloys.

3. SURFACE SEGREGATION IN ORDERED ALLOYS

Compared to SRO effects on surface segregation in solid solutions, the role of LRO should be naturally more prominent and common. Its elucidation requires calculations that take into account various factors contributing to the "net" segregation characteristics in ordered alloys including the temperature dependence: the crystal bulk structure and surface orientation, effective bulk and surface interatomic interactions (NN, non-NN) in relation to segregation driving forces, deviation from exact stoichiometry, possible surface relaxation and reconstruction, atomic vibrations, etc. This section attempts to quantify some of these factors and present several possible scenarios of segregation/order interplay.

Spatial ordering in the bulk of alloys and "classical" surface segregation in completely random solid solutions (without LRO or SRO) are both exothermic processes, which are enhanced at lower temperatures and accompanied by an entropy decrease. As discussed in our previous review [1] and mentioned in sec.1, their interplay in ordered alloys can completely modify the segregation behaviour resulting either in endothermic or exothermic surface segregation, depending primarily on the energy balance of the respective tendencies. In the former case segregation is hampered, and an increase in its equilibrium level with temperature can be expected due to the enhancement of compositional disorder that disrupts the near-surface LRO, and is associated with increased configurational entropy.

3.1 Prediction of order/segregation interplay by means of a simple model

As a first step, the interplay of surface segregation and long-range order in a binary alloy A_cB_{1-c} can be qualitatively evaluated by comparing the effective interaction strength (V) as a measure of ordering tendency with the "surface field" (Δh) reflecting the segregation basic driving force, similarly to the original approach of Moran-Lopes [2]. In this simple nearest-neighbour (NN) pair interaction model, as the "segregation/order factor", $r \equiv \left|\frac{\Delta h}{V}\right|$, gets larger the balance tips more towards segregation. To obtain more quantitative estimation of the effects, r has been used as a parameter in FCEM calculations for two types of ordered structures with ideally equiatomic bulk truncated surface, assuming segregation limited to the three outmost atomic layers.

3.1.1 Equiatomic binary alloys

Among possible equiatomic surfaces of equiatomic bulk alloys (e.g., B2(110), B32(110), and $L1_0$(111), see Fig.1) the calculations focused on bcc B2(110). For low or moderate values of r (<~10) a peaked segregation curve is predicted (Fig.6). Thus, starting with equiatomic bulk truncated composition at low temperatures, one of constituents (depending on sign of the non-zero surface field) segregates as disordering proceeds. At higher values of the ratio (r>~10) full monolayer is formed at low temperatures, and the segregation decreases with temperature monotonously (Langmuir-McLean type behaviour).

The role of bulk off-stoichiometry is exemplified in Fig.7. Even slight negative deviations diminish considerably segregation levels, while positive deviations lead to strong enhancement relative to the levels calculated for the exactly equiatomic bulk. These somewhat surprising findings can be understood in terms of the dominant bulk ordering tendency, by which excess atoms (>50%) are effectively pushed out from the bulk (due to its reduced coordination,

ordering tendency at the surface is weaker). This strong dependence of segregation on *small* deviations from the bulk stoichiometry should be taken into account in any analysis of ordered alloy segregation data (see below).

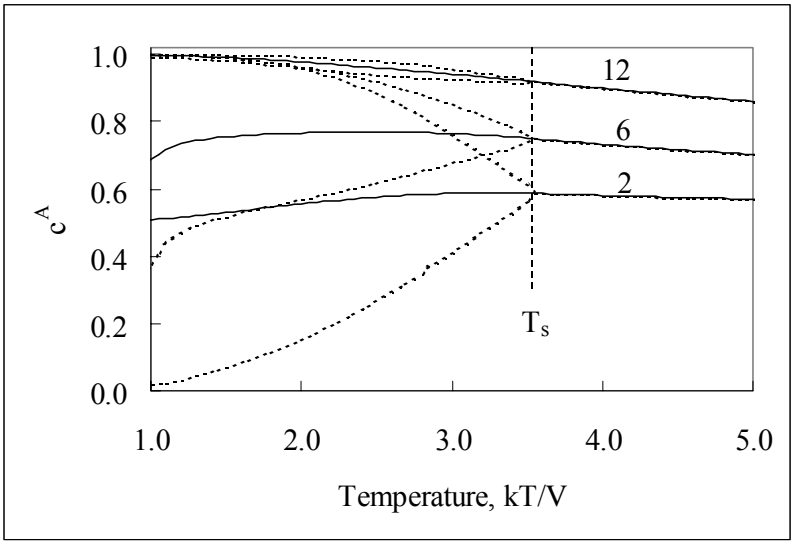

Fig.6. The B2(110) surface average (solid lines) and sub-lattice (dotted lines) concentrations of the segregant in AB model alloy as a function of reduced temperature calculated in the FCEM approximation for different segregation/order factors r (indicated near the plots). The difference in sub-lattice concentrations corresponds to the surface LRO parameter that vanishes at the surface transition temperature T_s that coincides with the bulk transition temperature T_b independently of r.

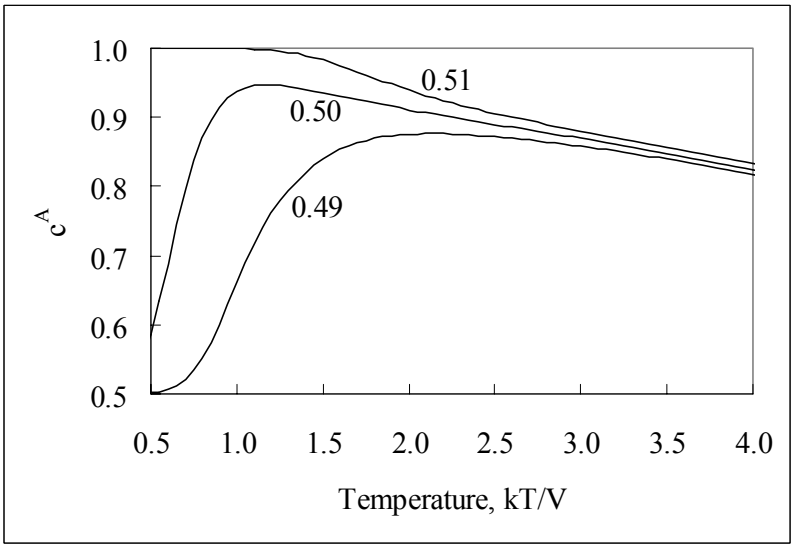

Fig.7. The B2(110) alloy surface average concentration as a function of temperature calculated in the FCEM approximation for model A_cB_{1-c} alloys with stoichiometric (c=0.50) and near-stoichimetric (c=0.49, 0.51) bulk concentrations (segregation/order factor r =8.9).

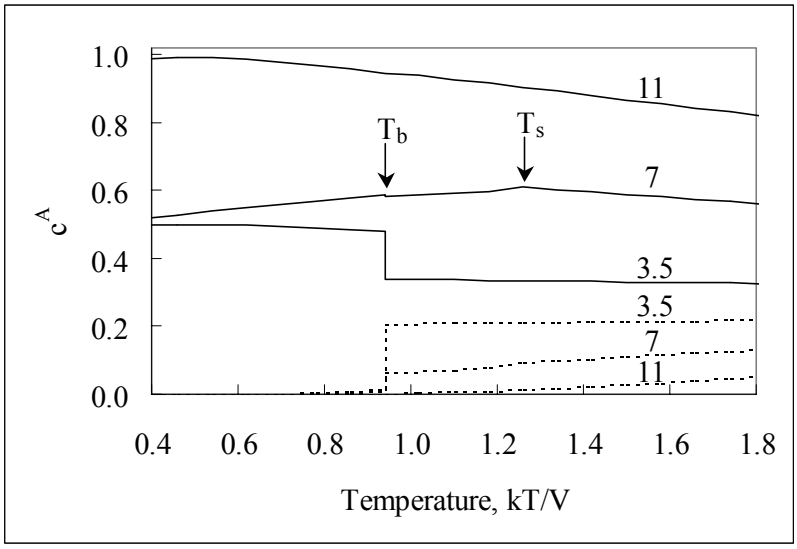

Fig.8. Variation with temperature of the average segregant concentration at the $L1_2(100)$ surface (solid lines) and at the first underlayer (dotted lines) in AB_3 model alloy calculated in the FCEM approximation for different segregation/order factors r (marked near the plots). Arrows indicate order-disorder transition temperatures (for r =3.5, T_s=T_b).

3.1.2 Non-equiatomic binary alloys

Another class of ideally bulk-truncated equiatomic surfaces of alloys (e.g., $L1_2(100)$ and $DO_3(100)$ with AB_3 bulk stoichiometry), exhibits more diverse segregation/order interplay compared to the previous class ("non-segregated", $c_S = c_B$, equiatomic termination). Because $c_S > c_B$, the segregation vs. temperature curve is not necessarily peaked. Equiatomic termination predicted for r<10 is followed by a peaked curve only for intermediate values of r (r>4.5) (Fig.8), but for lower r values (<4.5) a monotonous decrease below the equiatomic level is anticipated. At high values of the segregation/order factor (>~10), the behaviour resembles that of the previous class, namely, a full monolayer is formed at low temperatures, and then the segregation level monotonously decreases. Moreover, the diversity is manifested also by the

Table 2
Relationship of surface/bulk transition temperatures calculated for *$L1_2(100)$*

Segregation/order factor	Surface induced order/disorder or neither
r<2	$T_s < T_b$ (SID)
4> r >2	$T_s = T_b$
7.8>r>4	$T_s > T_b$ (SIO)
8>r>7.8	$T_s = T_b$
r>8	$T_s < T_b$ (SID)

disordering temperatures of the surface (T_S) vs. bulk (T_b). Depending on r, they can coincide, T_S can exceed T_b (surface-induced order, SIO), or be lower than T_b (surface-induced disorder, SID). SIO is promoted by surface compositions close to equiatomic (Fig.9), which correspond to intermediate values of the segregation/order factor, while SID occurs for high and low values of r, as shown in Table 2.

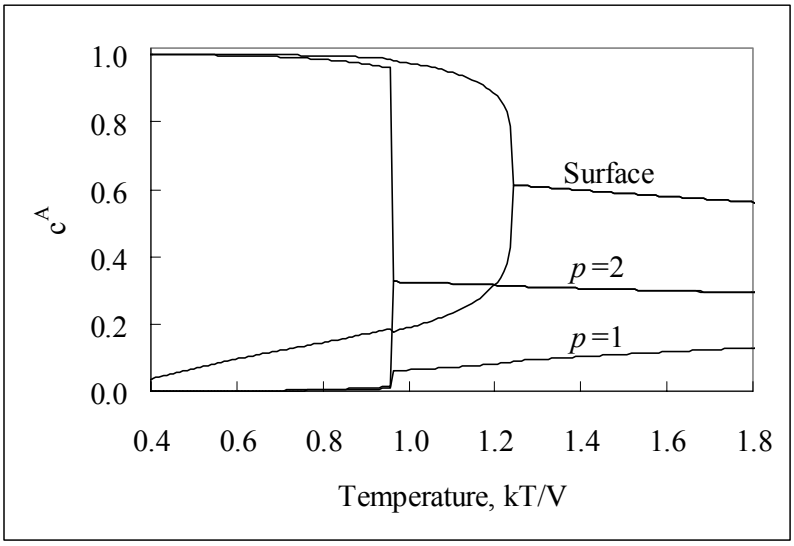

Fig.9. Surface Induced Order at the $L1_2(100)$ surface in AB_3 model alloy calculated in the FCEM approximation for r=7. p=1 and 2 correspond to the first and second under-layer, respectively.

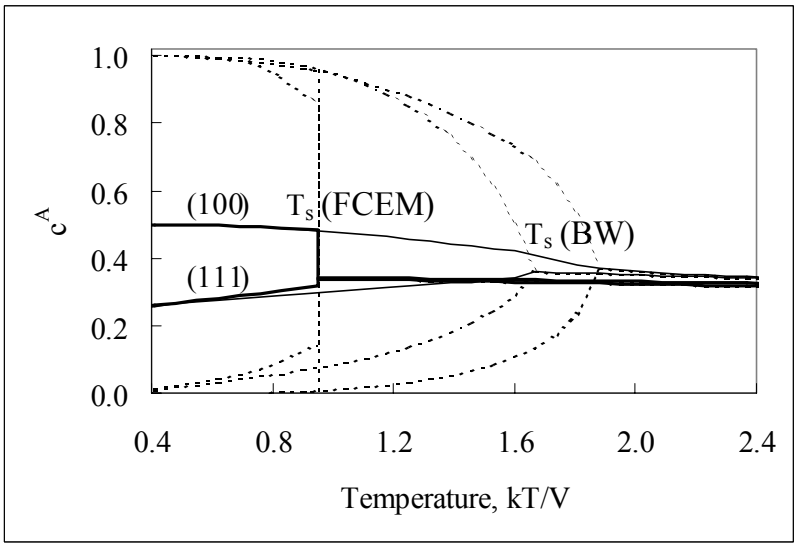

Fig.10. Average (solid lines) and sub-lattice concentrations (dotted lines) of $L1_2(100)$ and $L1_2(111)$ surfaces calculated in the BW and the FCEM approximations (thick lines) for r=3.5.

In addition to the segregation/order factor, and depending on its magnitude, the crystal structure and surface orientation can strongly affect the surface composition in ordered alloys. For example, unlike the case of the equiatomic bulk truncated composition of $L1_2(100)$, LRO tends to maintain the $L1_2(111)$ surface with nominal bulk concentration (0.25). Therefore, the two ordered surfaces are expected to exhibit quite different segregation characteristics for the same r value (Fig.10). Moreover, SRO causes pronounced changes of surface sublattice and average compositions associated with a considerable reduction of the order-disorder transition temperature (especially in fcc alloys).

3.2 Case studies

It is instructive to review order/segregation interplay in specific alloys in view of the diverse predictions furnished by the model calculations of the previous section. We have chosen to focus on the well-studied $Cu_3Au(100)$ surface, and to assess comparatively the segregation/order interplay in a large number of equiatomic aluminides. Pertinent theoretical and/or experimental recent findings for Cu_3Pd, Pt_3Sn and Co_3Pt are addressed too.

3.2.1 Compositional variations in $Cu_3Au(100)$ and $Cu_3Pd(110)$

The surfaces of Cu_3Au alloy (bulk structure $L1_2$) was studied thoroughly by various techniques and theoretical approaches, especially in relation to the order-disorder transition [52-63]. Recently, medium-energy ion-scattering spectroscopy (MEIS) measurements confirmed the stabilization of bulk-truncated equiatomic termination for this surface at low temperatures. Starting at about 500 K, the Au atoms in the surface layer begin to move to the second

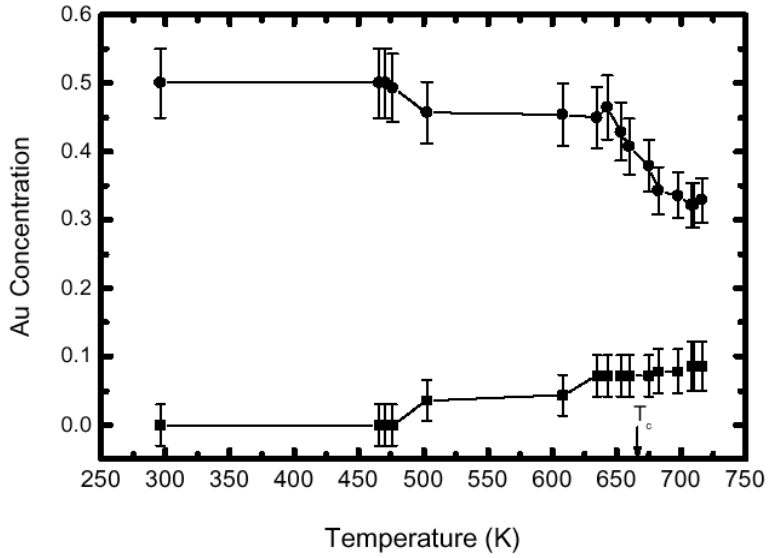

Fig.11. Variations in the atomic concentration of Au atoms in the first (●) and second (■) layer of $Cu_3Au(100)$ measured by MEIS as function of temperature [64].

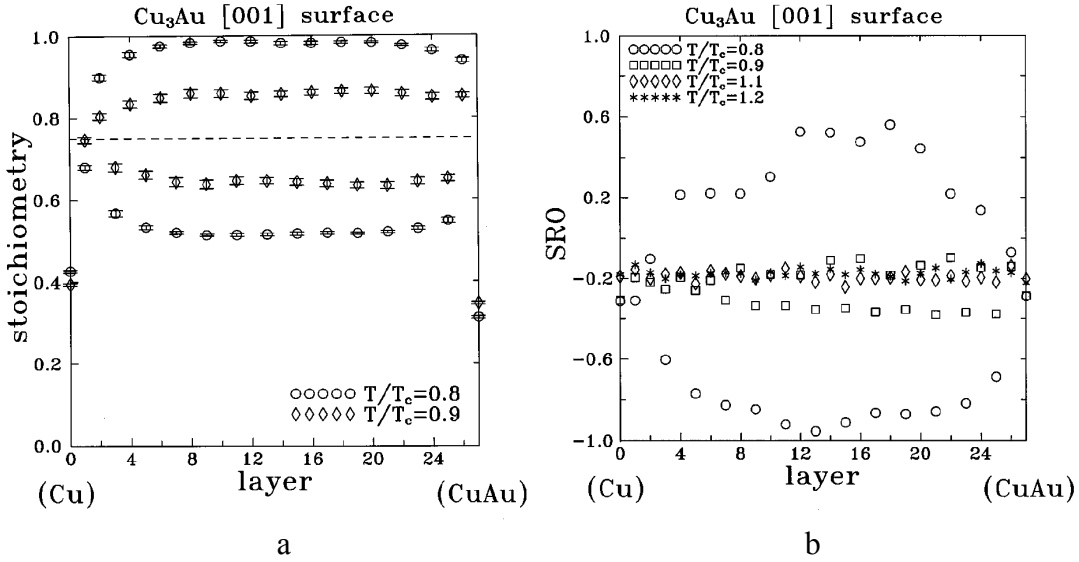

a b

Fig.12. (a) Plane-averaged stoichiometry profile of the (100) surfaces of Cu_3Au for T/T_c =0.8 and 0.9. (b) Short-range order for each plane parallel to the surfaces for T/T_c =0.8, 0.9, 1.1, and 1.2. Layer 0 corresponds to the Cu-terminated surface, and layer 27 to the CuAu-terminated surface (a simulation cell, $5\times5\times14$ in units of the lattice constant of Cu_3Au, with two free surfaces (100) was used). According to Ref.36.

layer (Fig.11), and their concentration decreases to 32% at 720 K. The surface and bulk disordering temperatures coincide, $T_S = T_b$ =663 K, [52,54,65]. These types of monotonously decreasing surface segregation and T_S/T_b relationship are consistent with the above model calculations of sec. 3.1.2 when $4>r>2$ (Table 2). Indeed, rough estimation of r based on V fitted to the bulk transition temperature, and Δh calculated from the constituent surface tensions and size mismatch energy, falls into this range.

More insight into equilibrium arrangements of atoms in the near surface region of this alloy was obtained by means of Monte Carlo simulations [36]. As is depicted in Fig.12a, inner layer concentrations oscillate according to the succession of the Cu planes and the CuAu planes. Cu concentrations of sub-surface layers converge to 0.75, which corresponds to the average concentration of the alloy and signifying near-surface disordering. Both truncations exhibit surface segregation of Au atoms, which is somewhat higher for the CuAu-terminated surface. Furthermore, while Au segregates mostly to the surface layer, the disorder is manifested in about six layers. The SRO characterized by the Cowley parameter* shown in Fig.12b behaves similarly to the LRO (Fig.12a). Below the transition SRO oscillates between negative values

* The Cowley SRO parameter is defined in this case as $\sigma = 1 - \frac{p_{Au}}{c_{Au}}$, where p_{Au} is the probability of finding Au atom at a site in the nearest-neighbor shell around a Cu atom [66].

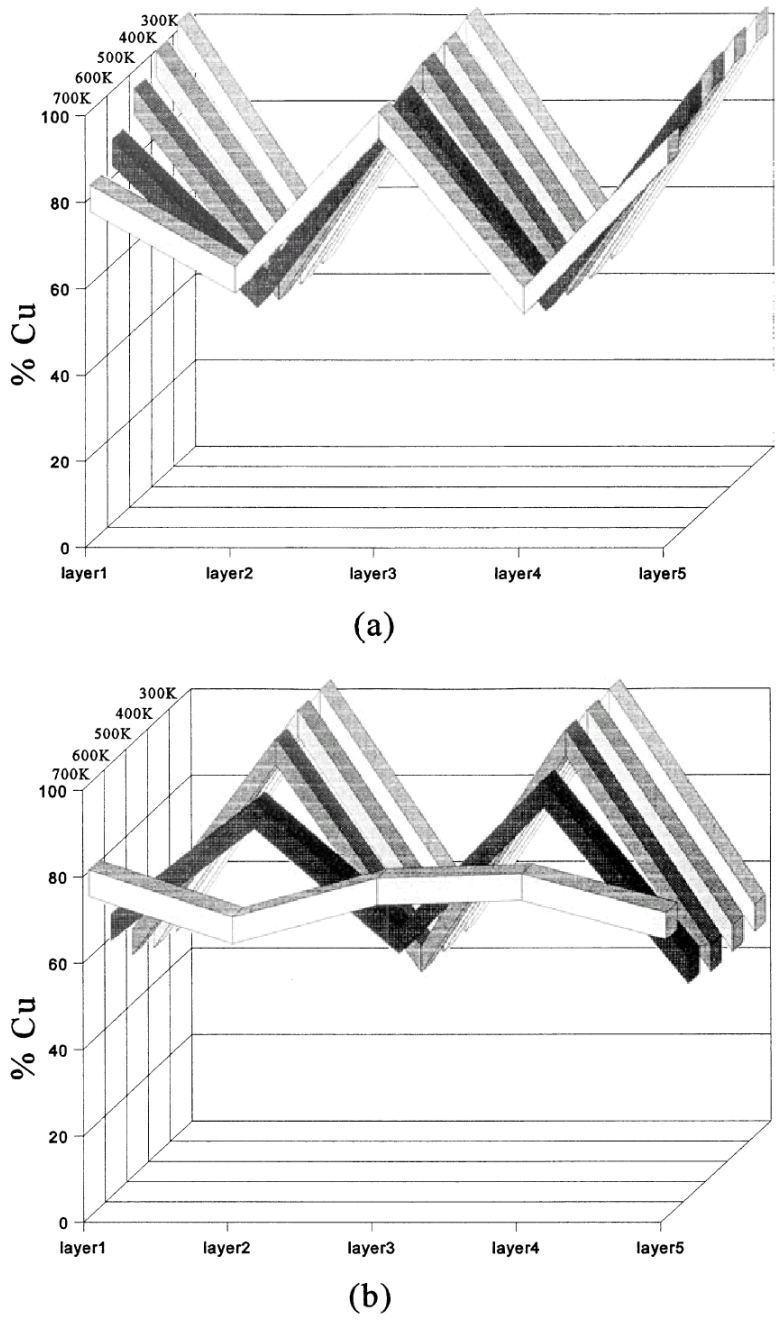

Fig.13. Concentration profiles for the Cu_3Pd alloy at different temperatures (300–700 K) in different Monte Carlo simulations [40]. (a) Simulation set S1 (b) simulation set S2. The EAM parameters used were optimized specifically for the Cu-Pd alloy.

in CuAu planes (preferred association of unlike atoms), and positive values in the Cu planes (preferred association of like atoms). Order that is maximal in the bulk-like layers gradually decreases near the surface, and for surface atoms with reduced coordination it drops close to the value (σ=-0.2) simulated for the bulk and the surface above T_C. The surface fraction of gold (~0.6), predicted in the simulations [32,36] and by electronic theory calculations [67] is somewhat

larger than should be in case of perfect bulk truncation (or measured experimentally [53,64], see Fig.11).

An opposite segregation trend, namely majority constituent segregation, is exhibited by $Cu_3Pd(110)$ surface, as revealed by LEIS [68]. The Cu segregation profile is oscillatory, and second layer ordering gave a (2×1) LEED pattern. Results of Embedded-Atom-Method Monte-Carlo (EAM-MC) simulations are in good agreement with the experimental findings [40]. Since along the [110] direction, the ordered Cu_3Pd bulk consists of alternating pure Cu and mixed CuPd layers, two sets of surface simulations were performed: a simulation set (S1) with pure Cu and another set (S2) with equiatomic CuPd termination (Fig.13). The former simulation set agrees better with experimental observations (note the predicted increase of surface Cu concentration with temperature in the second set).

3.2.2 Surface order in $Pt_3Sn(111)$ and Co_3Pt (111)

Deviations from bulk-like terminations are quite common in metallic alloys and can involve temperature dependent surface reconstructions, as well as SRO features different from those anticipated in the bulk. First, while the ideal bulk-like termination of the $L1_2(111)$ surface is the (2×2) structure, according to LEIS, AES and LEED measurements [69] annealing of sputtered $Pt_3Sn(111)$ leads to Sn-enriched $\sqrt{3}\times\sqrt{3}R30^\circ$ reconstruction, which gradually transforms at higher temperatures to the bulk-truncated (2×2) structure. At still higher temperatures, it transforms to a PtSn segregated $(2\times2)'$ new structure. Monte Carlo simulations combined with the "Macroscopic Atom" Model MAM [38] claim that the $\sqrt{3}\times\sqrt{3}R30^\circ$ structure is associated with preferential sputtering effects and the limited atomic mobility at the lower temperatures. (At higher temperatures the (2×2) ordered surface was predicted.) On the other hand, recent FCEM study [70] predicted stabilization of the $\sqrt{3}\times\sqrt{3}R30^\circ$ structure due to even slight bulk off-stoichiometry (<25% Sn). Moreover, assuming enhanced surface interactions ($V_S > V$) these calculations indicate stabilization of the $(2\times2)'$ reconstruction at the highest temperate range, just as observed experimentally [69].

The second case of non-bulk lateral ordering involves surface SRO. Scanning tunneling microscopy (STM) and quantitative LEED analysis of the (111) surface of disordered Co_3Pt alloy revealed SRO that differs from the type expected in the bulk having this composition ($L1_2$). In particular, Pt and Co atoms were found to be locally arranged in monoatomic chains with a (1×2) unit cell and nearly equiatomic composition, in a manner similar to the ordered $L1_0$ phase (Fig.14). Distortions needed for the tetragonal $L1_0$ phase explain why this surface ordering does not extend over larger domains [71]. The $Co_3Pt(111)$ SRO

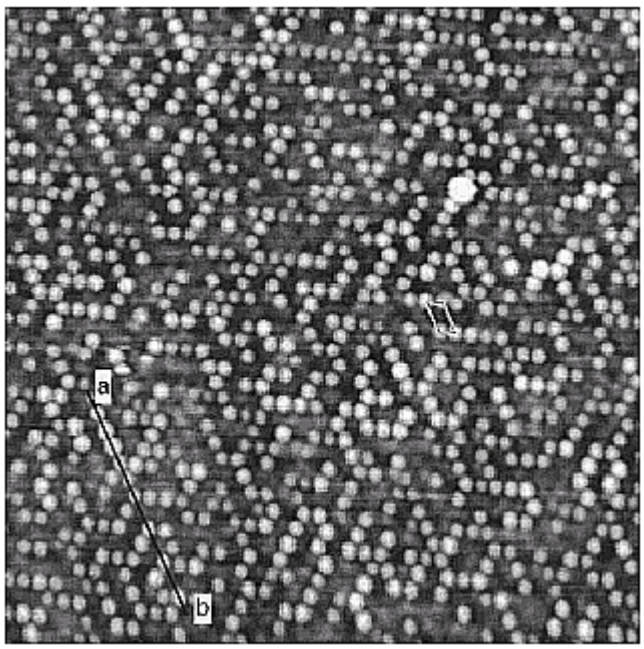

Fig.14. STM constant current topograph (10×10 nm, 0.5 mV, 3.8 nA) of $Co_3Pt(111)$ annealed at temperatures in the range 960–1060 K [71]. SRO appears as small areas with (1×2) symmetry in monoatomic chains. The bright spots are Pt sites.

parameters, quantitatively estimated by direct analysis of the STM images, indicate much stronger preference for unlike nearest neighbors compared to $Ni_3Pt(111)$ or $Rh_3Pt(111)$ [71-73].

3.2.3 Segregation characteristics of aluminide surfaces

FCEM calculations for three structurally different groups of equiatomic aluminides (B2(110), B32(110) and $L1_0(111)$) further demonstrate the decisive role of the segregation/order energetic factor r (Table 3). Surface-field related contributions, Δh, of the listed surfaces were estimated from the pure Al and second metal surface tensions [74] and lattice parameters were extracted from volume per unit formula data [75] (it was assumed that elastic strain contributions can be neglected in case of equiatomic composition). The interaction strengths were obtained from the corresponding heats of formation applying NN interaction model to B2 and $L1_0$ structures ($V = V_1, V_n = 0$ for $n > 1$). The B32 structure exhibits ordering also in the second coordination sphere, since NN and NNN interactions are comparable [76]. Therefore, it was treated assuming uniform interactions ($V = V_1 = V_2, V_n = 0$ for $n > 2$). As can be seen from Table 3, the heat of formation (and the corresponding effective interaction strength) of alloys with B2 structure, except for FeAl, is considerably higher than of alloys with the B32 and the $L1_0$ structures (it is least exothermic for aluminides of metals close to group 6 [77]).

Table 3
Energetic parameters of aluminum ordered alloys

Alloy	Structure/ Surface	Heat of formation*, (kJ/mol)	Interaction strength V**, meV	Surface field Δh, meV	$r = \left\lvert \frac{\Delta h}{V} \right\rvert$
ScAl	B2(110)	-84.6	218	14	0.064
CoAl	—"—	-63.8	165	566	3.4
NiAl	—"—	-67.3	174	455	2.6
RuAl	—"—	-58.2	150	905	6.0
RhAl	—"—	-89.3	231	674	2.9
FeAl	—"—	-28.6	74	660	8.9
CrAl	B32(110)	-11.7	24	363	15
MoAl	—"—	-22.9	47	746	16
TcAl	—"—	-19.2	40	830	21
TiAl	$L1_0$(111)	-37.2	96	629	6.5
VAl	—"—	-20.7	54	695	12.9
MnAl	—"—	-23.7	61	124	2.0

* From Ref.75
** Interaction strength in B2 and $L1_0$ is calculated in the NN approximation , while in B32 equal NN and next nearest neighbor (NNN) interactions are assumed.

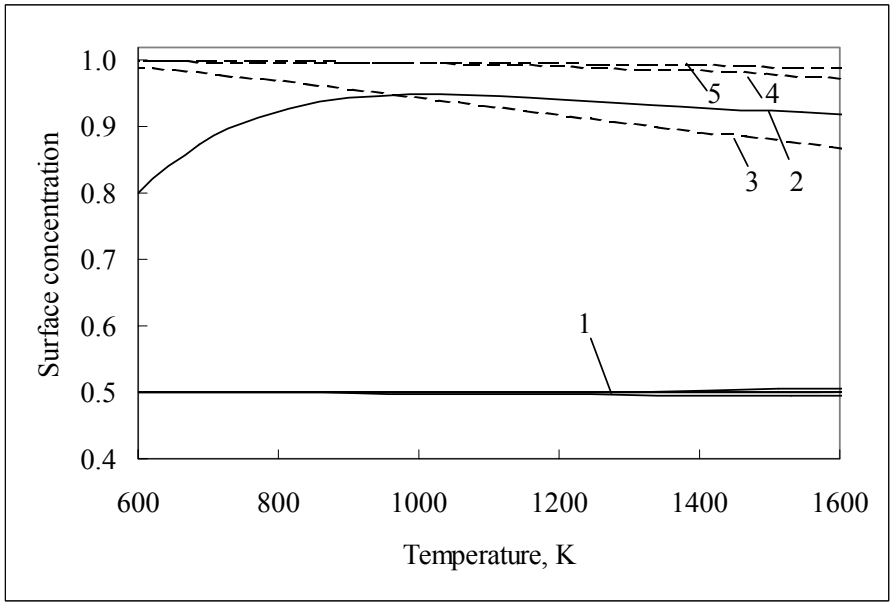

Fig.15. FCEM calculated variations with temperature in the average Al concentration at the (110) surface of bcc aluminides (B2 structure - solid lines, B32 structure - dashed lines). 1 - ScAl, RuAl, RhAl, NiAl, CoAl, 2 - FeAl, 3 - CrAl, 4 - MoAl, 5 - TcAl. The surface concentrations were calculated in accordance with data of Table 3.

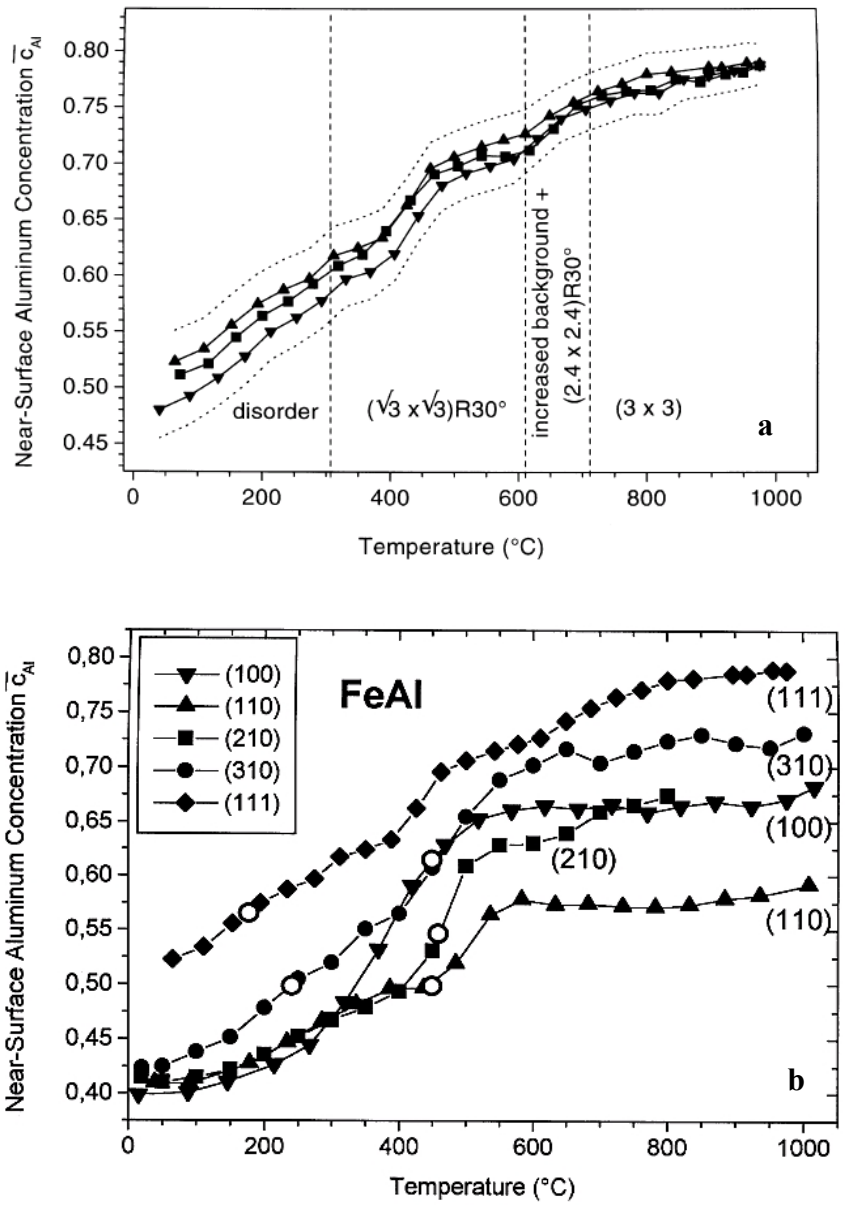

Fig.16. (a) AES determined near-surface (average) concentration of Al as function of annealing temperature for the FeAl(111) surface (three datasets). The dotted lines estimate the uncertainty introduced by the error in the matrix factor. The phases, which are observed in LEED after quenching the annealed sample to room temperature, are also shown. (b) Comparison of the segregation curves for all investigated surface orientations. Near-surface concentrations corresponding to bulk terminated surfaces are marked by open circles [77].

These energetic parameters were used in FCEM calculations assuming segregation at the three outmost layers only. As shown in Fig.15, the segregation tendency prevails only in the B32 ordered alloys and the surface concentration decreases with temperature (entropy-driven monotonous desegregation). This behavior is associated with the distinctly high segregation/order factor (sec. 3.1). On the other hand, ordered bulk truncation with surface concentration very

slightly increasing with temperature is predicted for most of the B2 ordered alloys. Only in FeAl, with relatively low heat of formation and intermediate r value, there is a subtle balance between segregation and order, leading to a peaked segregation curve in experimentally accessible range of temperatures. Indeed, as measured by AES and LEED, the behavior of the FeAl(110) [77] differs substantially from the equivalent surfaces of alloys with NiAl and CoAl like energetic parameters, which exhibit nearly perfect stoichiometry at the top layer (bulk truncation) [78-80]. The predicted surface segregation increase in FeAl with annealing temperature was observed [77] also for other surface orientations and was accompanied by surface reconstructions (Fig.16). The calculations for the strictly stoichiometric FeAl alloy predict somewhat higher segregation levels (Fig.15) compared to the reported formation of incommensurate $FeAl_2$ surface alloy on the FeAl(110) surface [77]. The discrepancy can be due, at least partially, to a slight deviation from stoichiometry in the measured alloy (see Fig.7).

As an example for a third class of equiatomic aluminides, calculations done for three fcc $L1_0$ alloys are presented in Fig.17. Again, the segregation behavior is governed mainly by the segregation/order interplay, as expressed by means of r (see Table 3). Only in VAl with relatively high r value (12.9), the segregation tendency prevails.

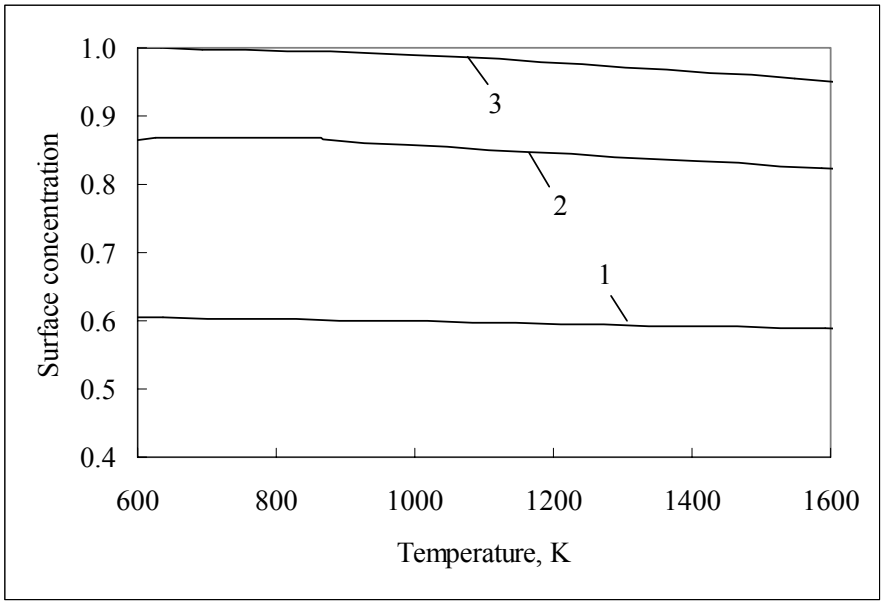

Fig.17. FCEM calculated variations with temperature in the average Al surface concentration at the (111) surface of fcc $L1_0$ aluminides. 1 - MnAl, 2 - TiAl, 3 - VAl. The surface concentrations were calculated in accordance with data of Table 3.

4. Segregation in a bi-phase binary alloy

As discussed in previous sections the involvement of ordering effects in binary alloy surface segregation complicates its theoretical treatment. Unraveling segregation phenomena in multi-component alloys is another challenge. But the situation can become even more complex for segregation in multi-phase alloys, when distinct segregation processes from individual bulk phases are coupled to the temperature dependent phase equilibria (Fig.18) In particular, in many binary alloy systems with ordering tendency bi-phase equilibrium exists between a solid-solution and an ordered compound when the bulk concentration exceeds the solubility limit (Fig.18). As discussed below, besides segregation/LRO-SRO effects that can be operative in each phase separately, the variations with temperature in the solid-solution bulk composition can have a dominant effect and also lead to peaked segregation curves.

Such a behavior, as measured by means of XPS, was reported previously for fcc-based Al-3%Ag alloy equilibrated between 550 and 770 K [82] (Fig.19a). Below the bulk phase transition (680 K) hcp-based Ag_2Al-like

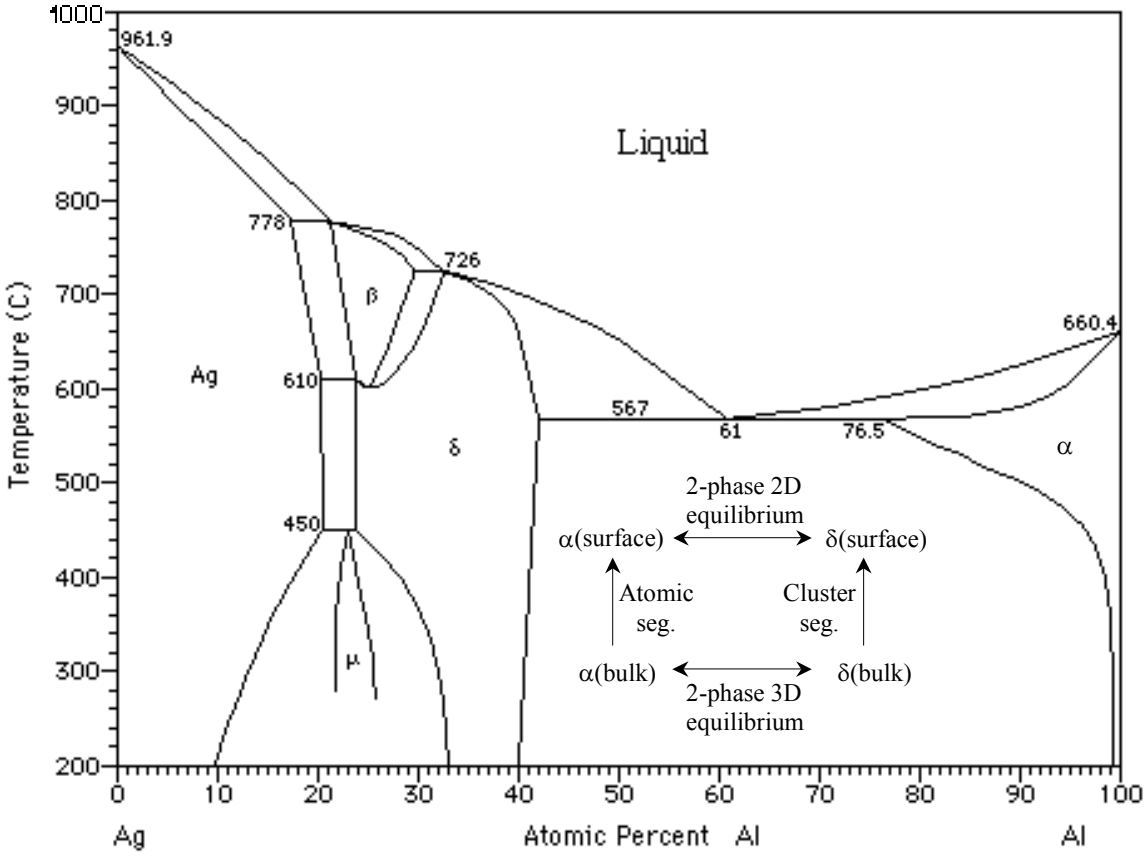

Fig.18. Phase diagram of Al–Ag [81]. Insert: schematics of processes pertinent to surface segregation in bi-phase alloys (α – solid solution, δ – ordered compound).

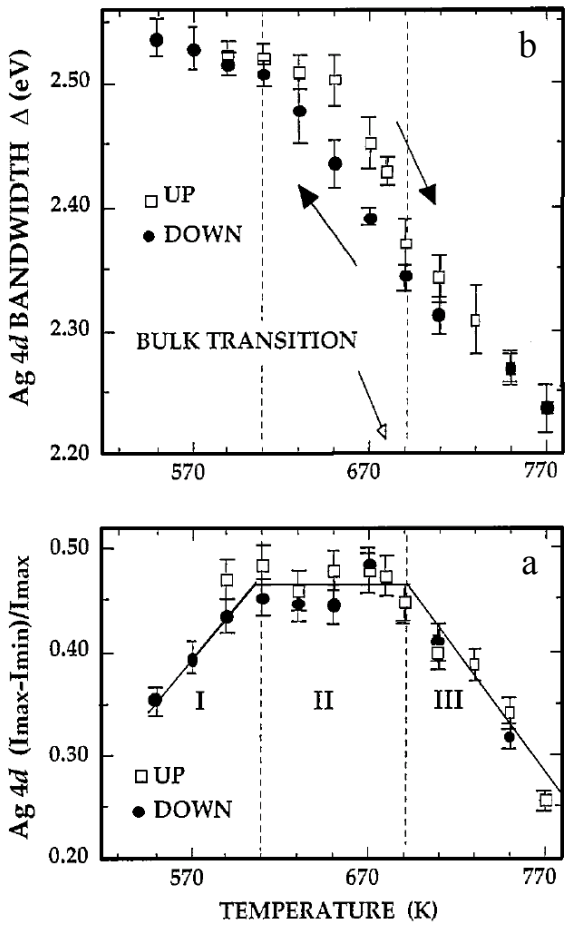

Fig.19. The XPS bandwidth of the Ag 4d states in Al-3at.%Ag (top) and the Ag concentration (bottom), deduced from the emission intensity, as a function of temperature [82]. The bulk phase transition lies at 680 K.

clusters (δ-phase) precipitate in the fcc solid solution α (Fig.18). Evidence for the appearance of (111) surface clusters came from secondary electron imaging (SEI), Fig.20. In addition, changes in the Ag 4d linewidth (Fig.19b) were attributed to varying numbers of Ag neighbors of a given Ag atom, and thus were supposed to reflect the relative extent of clustering vs. Ag dissolved in the Al matrix. Based on these data, the three regions in the segregation curve (Fig.19a) were tentatively attributed to:

i) Segregation enhancement of small Ag_2Al-like clusters with increasing temperature;

ii) Their gradual dissolution (first-order phase transition), without a change in the overall concentration of Ag atoms in the analyzed volume (610-690K), and

iii) Ag atom desegregation at higher temperatures.

Recently, an attempt was made to analyze the compositional changes in a quantitative manner and so to elucidate the pertinent mechanism in terms of the

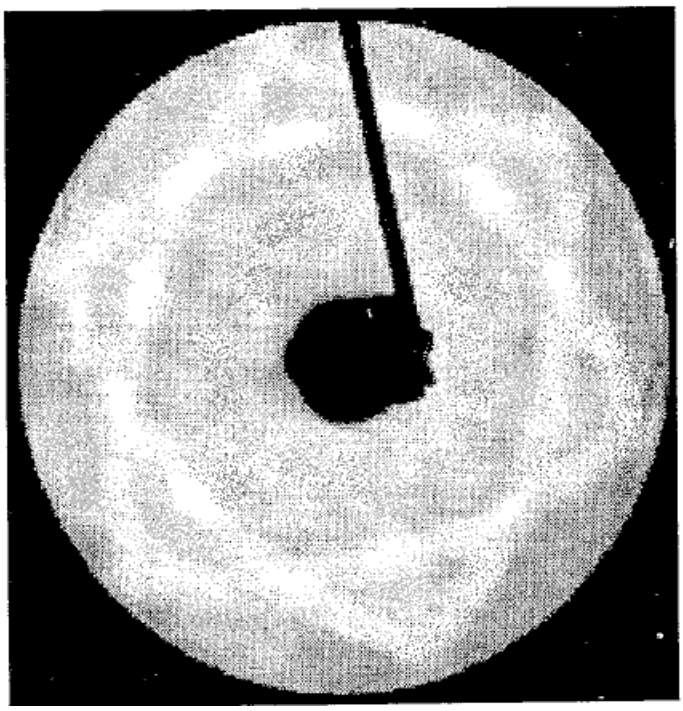

Fig.20. Secondary-electron imaging (SEI) pattern obtained from epitaxial Ag on Al(111) heat treated at 410 K. The sixfold symmetry verifies the formation of Ag_2Al clusters with hcp structure [82].

two-phase bulk equilibrium as well as the involvement of two distinct segregation routes, that of atomic Ag and of Ag_2Al clusters [83]. In principle, since the formation of ordered phase clusters at lower temperatures is accompanied by a reduction in Ag solute concentration in the bulk of the solid solution, surface segregation from the latter is suppressed. As temperature increases, gradual dissolution of bulk clusters results in increase in bulk and surface Ag concentration of the solid solution matrix. Around the phase transition (crossing the solubility line), when the solid-solution composition becomes constant with temperature (3%Ag), the surface concentration starts to decrease monotonously as is common in random solid solutions (McLean-Langmuir entropy driven desegregation). More quantitatively, the Ag concentration c_α of the bulk solid solution can be simply evaluated from the relevant portion of the Al-Ag phase diagram (Fig.18). For a given Ag overall atomic concentration (c), c_α increases with temperature (concomitantly with decreasing amounts of the δ-phase clusters) according to the solubility line approximate formula

$$c_\alpha = A \exp\left(-\frac{\lambda}{kT}\right). \tag{6}$$

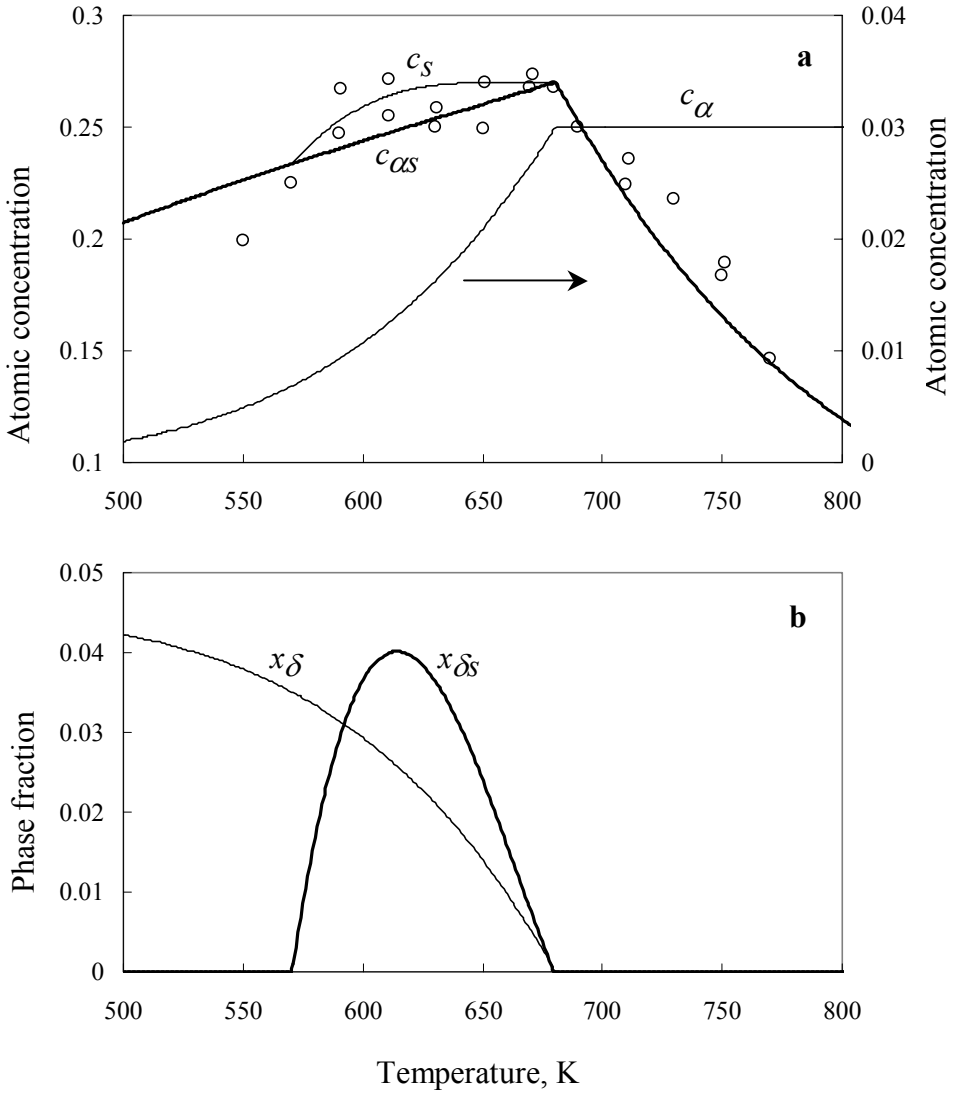

Fig.21. Segregation temperature dependence in the bi-phase Al-3%Ag alloy: (a) The surface concentration of the solid solution phase ($c_{\alpha S}$), based on the depicted c_α curve. Circles: average surface concentration derived from experimental data of Ref.82 (as in Fig.19a) and c_S is the best-fit line. (b) The bulk fraction x_δ and surface fraction $x_{\delta S}$ of the Ag_2Al clusters, derived from c_α and $c_S - c_{\alpha S}$, respectively.

Fitting this equation to Al(Ag) solubility experimental data in the temperature range from 573 to 773 K [84] gives $A \approx 62.2$ and $\lambda \approx 43.0$ kJ/mol. The monotonous increase in c_α with temperature is depicted in Fig.21a, and the corresponding decreasing δ-phase fraction (lever rule) in Fig.21b.

Eq.6 with these parameters together with the apparent segregation excess enthalpy $\Delta H_{seg} = -38.5$ kJ/mol and segregation excess entropy $\Delta S_{seg} = 36.1$

kJ/mol/K (as deduced by Lee et al [85] from experimental data on Ag segregation in Al-4.2%Ag) have been used for a Langmuir-McLean type calculation of monolayer segregation levels from the Al-3%Ag solid solution ($c_{\alpha s}$), including the two-phase region (Fig.21a),

$$\frac{c_{\alpha s}}{1-c_{\alpha s}} = \frac{c_{\alpha}}{1-c_{\alpha}} \exp\left(-\frac{\Delta H_{seg}}{kT} + \frac{\Delta S_{seg}}{k}\right). \qquad (7)$$

Since $\left|\Delta H_{seg}\right| < \lambda$ and the value of c_{α} given by eq.5 with the parameters for this system is small, $c_{\alpha s}$ increases with temperature (Fig.21a). Namely, in the solubility/segregation "competition" the solubility factor prevails, and the overall process energetics is endothermic.

According to the experimental data [82] clusters disappear from the surface close to the temperature of bulk transition, $T_b \approx 680$ K for $c = 0.03$, so the average surface concentration c_s below this temperature (Fig.21) contains in addition to "freely" segregated Ag atoms, also contributions of the clusters with fraction $x_{\delta s}$. It is calculable from the measured (average) surface composition,

$$c_s = x_{\delta s} c_{\delta} + (1 - x_{\delta s}) c_{\alpha s}. \qquad (8)$$

The values $x_{\delta s}$ derived from the experimental c_s and calculated $c_{\alpha s}$ values (Fig.21b) exhibit a distinct peaked dependence on temperature with maximal surface fraction pertaining to the δ-phase at ~70 K below T_b.

Questions regarding possible kinetic limitations at the low temperature range [83], the mechanism and driving forces for cluster segregation, and the possibility of clustering/ordering due to segregating Ag atoms (drawn schematically in Fig.18) remain open.

This approach can be applied to segregation phenomena in other two-phase alloys, such as reported recently for polycrystalline $Fe_{99}Pd_1$ with a small fraction of ordered FePd nuclei [86]. Positive entropy and enthalpy characterize the observed increase in segregation level with temperature.

5. SUMMARY

This review was aimed at elucidating some recent developments regarding surface segregation phenomena in metallic alloys exhibiting appreciable compositional order. It comprises three main issues: (i) short range order (SRO) effects in multi-component solid solutions, (ii) the role of long range order, LRO (with emphasis on the underlying energetics), and (iii) preliminary analysis of

segregation trends characteristic of bi-phase alloys. For qualitative and quantitative estimation of segregation/order interplay the statistical-mechanical "Free Energy Concentration Expansion Method" (FCEM), that uses simple pair bond energetics but takes into account SRO analytically, appears to be most convenient, and demands much less computational effort than Monte Carlo simulations, examples of which are presented too.

In the first issue (sec.2) the FCEM formulas were extended to the case of alloys with any number of components and were applied to the elucidation of effects of interatomic interactions and SRO on surface segregation in Ni-8%Al-4%Cu as a model ternary solid solution. The calculations revealed strong, SRO enhanced Cu segregation/Al+Ni desegregation in a site competition process that is largely attenuated following a compositional phase transition. The FCEM analytical formulas are applicable to surface segregation in semi-infinite alloys with any number of components, as well as to thin films and nano-particles, allowing systematic studies of SRO effects in these systems.

In the second issue (sec.3) several factors pertinent to segregation LRO (and SRO) induced modifications (mainly suppression) are addressed. Besides structural factors such as the surface orientation, the energy balance between the two tendencies plays a decisive role in most phenomena, and can be simply expressed by means of its numerical ratio (the "segregation/order factor", r). According to the FCEM model calculations for alloys with large ratio (e.g., $r > \sim 10$) segregation should prevail and exhibit a monotonous decrease with temperature typical to random solid solutions, whereas for low r values order is expected to dominate and segregation should be strongly or even completely inhibited. In the most interesting case of alloys with intermediate r values, representing a subtle balance of the two tendencies, a peaked segregation vs. temperature dependence is expected. Depending on the alloy energetics (r) and crystal structure, the surface transition temperature can either coincide with the bulk one, or be higher (surface-induced order, SIO), or lower (surface-induced disorder, SID). Experimental studies of equiatomic aluminides and Cu_3Au are in general agreement with the predictions. Another factor manifested in the segregation/order interplay involves ordered alloys with slight off-stoichiometry, where the tendency for a perfectly ordered bulk enhances segregation of the element in excess.

While both LRO and SRO effects on segregation are determined largely by the energetic balance as reflected by the magnitude of r, the role of LRO is naturally more prominent, and thus received more attention in this review. Yet, as exemplified for the above mentioned ternary solid solution, SRO associated with appreciable solute-solvent interactions can affect considerably surface compositional phase transitions. Likewise, in ordered fcc alloys with both LRO and SRO operative, order-disorder surface phase-transition temperatures are significantly shifted by SRO, thus modifying the individual sub-lattice

concentrations and the *average* surface composition. Another aspect briefly addressed deals with the nature of in plane surface atomic order. Several cases of deviations from the bulk truncated surface order of the long range type (surface reconstruction), and surface modified SRO are demonstrated.

Order/segregation interrelations, in their more general sense, can become even more complex in multi-phase alloys, when distinct surface segregation processes from individual bulk phases may be coupled to temperature dependent phase equilibria. Bi-phase systems, comprising of ordered clusters in a solid solution matrix, can exhibit two distinct but interrelated routes, namely, elemental segregation from the solid solution and segregation of small clusters. It is demonstrated for Al-3%Ag (sec.4) that variations with temperature in the solid-solution bulk composition alone can have a dominant effect leading to peaked segregation-temperature curves too. As many metallic alloys of practical importance are both multi-element and multi-phase, extension of this preliminary theoretical analysis seems to be desirable.

Finally, it should be noted that compared to a prominent theoretical progress in elucidating trends associated with segregation/order interplay by means of FCEM calculations (or by the generally more accurate Monte Carlo simulations with embedded-atom-method energetics), comprehensive experimental studies of the phenomena are still lacking. It can be anticipated that the growing use of advanced techniques sensitive to the atomistic features of surface structural order and composition will be directed to further unraveling of segregation/order issues.

REFERENCES

[1] M. Polak and L. Rubinovich, Surf. Sci. Rep., 38/4-5 (2000) 127.
[2] J. L. Moran-Lopez and L.M. Falicov, Phys. Rev., B 18 (1978) 2542.
[3] M. Polak, J. Deng and L. Rubinovich, Phys. Rev. Lett., 78 (1997) 1058.
[4] S. Hofmann and P. Lejcek, Colloque de physique, 51 (1990) C1-179.
[5] E. Taglauer, (private communication 1998).
[6] P. Weinberger, V. Drchal, L. Szunyogh, J. Fritscher, B. I. Bennett, Phys. Rev., B 49 (1994) 13366.
[7] S. Dorfman, V. Liubich, D. Fuks, Intern. Journ. of Quant. Chem., 75 (1999) 927.
[8] I. Mirebeau, M. Hennion and G.Parette, Phys. Rev. Lett., 53 (1984) 687.
[9] M. Polak, C.S. Fadley, L. Rubinovich, Phys. Rev B (in press).
[10] D. McLean, Grain Boundaries in Metals, Oxford University Press, London, 1957.
[11] J. L. Moran-Lopez and K. H. Bennemann, Phys. Rev., B 15 (1977) 4769.
[12] M.J. Sparnaay, Surf. Sci. Rep., 4 (1984) 101.
[13] V. Kumar and K. H. Bennemann, Phys. Rev. Lett., 53 (1984) 278.
[14] J.M. Sanchez, J.L. Moran-Lopez, Phys. Rev., B 32 (1985) 3534.
[15] J.M. Sanchez, J.L. Moran-Lopez, Surf. Sci. Lett., 157 (1985) L297.
[16] J.M. Sanchez, J.L. Moran-Lopez, Statistical Thermodynamics of Surfaces and Interfaces, in Nanophases and Nanocrystalline Structures, R.D. Shull and J.M. Sanchez Eds., A publication of TMS, Warrendale, Pennsylvania, 1993.

[17] Y. Teraoka, Surf. Sci., 242 (1991) 113.
[18] A.V. Ruban, I.A. Abrikosov, D.Ya. Kats, D. Gorelikov, K.W. Jacobsen and H.L. Skriver, Phys. Rev., B 49 (1994) 11383.
[19] J.M. Roussel, A. Saul, L. Rubinovich and M. Polak, J. of Phys.: Cond. Matt., 11 (1999) 9901.
[20] L. Rubinovich and M. Polak, Surf. Sci. (submitted for publication).
[21] F.F Abraham and C.R. Brundle, J. Vac. Sci. Technol. 18(2) (1981) 506.
[22] M.S. Dow, M.I. Daskes, Phys. Rev., B 29 (1984) 6443.
[23] S.M. Foiles, Phys. Rev., 32 (1985) 7685.
[24] S.M. Foiles, Calculation of the surface segregation of alloys using the embedded atom method in: P. A. Dowden and A. Miller Eds. Surface segregation phenomena, CRC, Boston, 1990.
[25] S.M. Foiles, M.I. Baskes and M.S. Daw, Phys. Rev., 33 (1986) 7983.
[26] J. Tersoff, Phys. Rev., B 42 (1990) 10965.
[27] H. Stadler, W. Hofer, M. Schmid and P.Varga, Phys. Rev., B 48 (1993) 11352.
[28] H.Y. Wang, R. Najafabadi, D.J. Srolovicz, R. LeSar, Phys. Rev., B 45 (1992) 12028.
[29] R. Najafabadi and D. J. Srolovitz, Surf. Sci., 286 (1993) 104.
[30] A. Saul, B. Legrand, G. Treglia, Phys. Rev., B 50 (1994) 1912.
[31] G. Bozzolo, B. Good, J. Ferrante, Surf. Sci., 289 (1993) 169.
[32] M. Hou, M. El Azzaoui, Surf. Sci., 380 (1997) 210.
[33] K. Binder, Phase transitions at surfaces. In: Cohesion and Structure of Surfaces ED D.G. Pettifor. Elsevier Science B.V., 1995.
[34] P. Wynblatt and A. Landa, Comp. Mater. Sci., 15 (1999) 250.
[35] B. Good, G.H. Bozzolo and P.B. Abel, Surf. Sci., 454/456 (2000) 602.
[36] A. Maidou and H. M. Polatoglou, Phys. Rev., B 60 (1999) 9145.
[37] C. Creemers and P. Deurinck, Surf. Interface Anal., 25 (1997) 177.
[38] C. Creemers, S. Helfensteyn, Appl. Surf. Sci., 167 (2000) 216.
[39] M. I. Baskes, Phys. Rev., B 46 (1992) 2727.
[40] P. Deurinck, C. Creemers, Surf. Sci., 419 (1998) 62.
[41] U. Bardi, Rep. Prog. Phys., 57 (1994) 39.
[42] M. Guttmann, Metall. Trans. 8A (1977) 1383; M. Guttmann and D. McLean, in: Interfacial Segregation, Eds. W.C. Johnson and J.M. Blakely, ASM, Metals Park, OH, 1979, p.261.
[43] M.A. Hoffmann and P. Wynblatt, Metall. Trans., 20A (1989) 215.
[44] W.C. Cheng and P. Wynblatt, Surf. Sci., 364 (1996) 409.
[45] M.A. Krivoglaz and A.A. Smirnov, The Theory of Order-Disorder in Alloys, Macdonald, London, 1964.
[46] R V Chepulskii y and V N Bugaev, J. Phys.: Condens. Matter, 10 (1998) 7309.
[47] C.H.P. Lupis, J. F. Elliott, Acta Met. 14 (1966) 1019; C.H.P. Lupis, Chemical Thermodynamics of Materials, North-Holland, New York-Amsterdam-Oxford, 1982.
[48] G. Treglia, B. Legrand, P. Maugain, Surf. Sci. 225 (1990) 319.
[49] O. Kubaschewski and C. B. Alcock, Metallurgical Thermochemistry. Pergamon, Oxford, 1979.
[50] M. Polak, M. Talianker, R. Arkush, Surf. Sci., 273 (1992) 363.
[51] M. Polak, L. Rubinovich, Surf. Sci., 377 (1997) 1019.
[52] V.S. Sundaram, B. Farrell, R.S. Alben, and W.D. Robertson, Phys. Rev. Lett., 31 (1973) 1136.
[53] T.M. Buck, G.H. Wheatley, and L. Marchut, Phys. Rev. Lett., 51 (1983) 43.
[54] E.G. McRae and R.A. Malic, Surf. Sci., 148 (1984) 551.

[55] K.D. Jamison, D.M. Lind, F.B. Dunning, and G.K. Walters, Surf. Sci. Lett., 159 (1985) L451.
[56] S.F. Alvarado, M. Campagna, A. Fattah, and W. Uelhoff, Z. Phys., B 66 (1987) 103.
[57] H. Dosch, L. Mailander, A. Lied, J. Peisl, F. Grey, R.L. Johnson, and S. Krummacher, Phys. Rev. Lett., 60 (1988) 2382.
[58] E.G. McRae and T.M. Buck, Surf. Sci., 227 (1990) 67.
[59] H. Dosch, L. Mailander, H. Reichert, J. Peisl, and R.L. Johnson, Phys. Rev., B 43 (1991) 13172.
[60] H. Reichert, P.J. Eng, H. Dosch, and I.K. Robinson, Phys. Rev. Lett., **7**4 (1995) 2006.
[61] H. Niehus and C. Achete, Surf. Sci., 289 (1993) 19.
[62] H. Niehus, Phys. Stat. Sol., B 192 (1995) 357.
[63] F.M. Zhang, B.V. King, and D.J. O'Connor, Phys. Rev. Lett., **7**5 (1995) 4646.
[64] D.H. Oh, H.J. Kang, K.H. Chae, C.N. Whang, B.V. King, D.J. O'Connor and D.W. Moon, Surf. Sci., 477 (2001) L289.
[65] Mannori C, Boato G, Canepa M, Cantini P, Mattera L, Terreni S, Europhys. Lett., 45 (1999) 686.
[66] J.M. Cowley, J. Appl. Phys. 21 (1950) 24; Phys. Rev., **7**7, 669 (1950).
[67] Y.C. Yong, H.C. Poon, Surf. Sci., 338 (1995) L825.
[68] R.H. Bergmans, M. van de Grift, A.W. Denier van der Gon, H.H. Brongersma, Surf. Sci., 345 (1996) 303.
[69] W.C.A.N. Ceelen, A.W. Denier van der Gon, M.A. Reijme, H.H. Brongersma, I. Spolveri, A. Atrei, U. Bardi, Surf. Sci., 406 (1998) 264.
[70] M. Polak and L. Rubinovich, to be published.
[71] Y. Gauthier, R. Baudoing-Savois, J.M. Bugnard, W. Hebenstreit, M. Schmid, P. Varga, Surf. Sci., 466 (2000) 155
[72] M. Schmid, H. Stadler, P. Varga, Phys. Rev. Lett., 70 (1993) 1441.
[73] E.L.D. Hebenstreit, W. Hebenstreit, M. Schmid, P. Varga, Surf. Sci., 441 (1999) 441.
[74] L.Z.Mezey and J. Giber, Jap. J. App. Phys., 21 (1982) 1569.
[75] D. Nguyen-Manh, D.G. Pettifor, Intermetallics, 7 (1999) 1095.
[76] L.M. Rubinovich, D.M. Stern, E.V. Kozlov, Izv. Vuz. Fiz., 32 (1989) 11 (in Russian). Translation: Sov. Phys. J., 32 (1989) 588.
[77] L. Hammer, H. Graupner, V. Blum, K. Heinz, G.W. Ownby, D.M. Zehnerb, Surf. Sci., 412/413 (1998) 69.
[78] H.L. Davis, J.R. Noonan, Phys. Rev. Lett., 54 (1985) 566.
[79] D.R. Mullins, S.H. Overbury, Surf. Sci., 199 (1988) 141.
[80] V. Blum, C. Rath, G.R. Castro, M. Kottcke, L. Hammer, K. Heinz, Surf. Rev. Lett., 3 (1996) 1409.
[81] T.B. Massalski, et al., Binary Alloy Phase Diagrams, 2 ed., OH, ASM Int.: Materials Park, 1990.
[82] M. Erbudak, M. Hockstrasser and E. Wetli, J. Electron Spectr. Related Phenom., 76 (1995) 529.
[83] M. Polak and L. Rubinovich, to be published.
[84] M. Hansen, K. Anderko, Constitution of Binary Alloys, New York, Mcgraw-Hill, 1958.
[85] H.K. Lee, R.W. Hyland, H.I. Aaronson, P.P. Wynblatt, Surf. Sci., 408 (1998) 288.
[86] C. Creemers, Surf. Sci., 360 (1996) 10.